Published in final edited form as:
Biomaterials. 2014 April ; 35(11): 3489–3496. doi:10.1016/j.biomaterials.2014.01.027.

FRET-enabled Biological Characterization of Polymeric Micelles

Stephen W. Morton[a,b,‡], **Xiaoyong Zhao**[a,‡], **Mohiuddin A. Quadir**[a], and **Paula T. Hammond**[a,b,c,*]

[a,*]David H. Koch Institute for Integrative Cancer Research, Massachusetts Institute of Technology, 77 Massachusetts Avenue, Cambridge, MA 02139

[b]Department of Chemical Engineering, Massachusetts Institute of Technology, 77 Massachusetts Avenue, Cambridge, MA 02139

[c]Institute for Soldier Nanotechnologies, Massachusetts Institute of Technology, 77 Massachusetts Avenue, Cambridge, MA 02139

Abstract

Translation of micelles from the laboratory to the clinic is limited by a poor understanding of their *in vivo* fate following administration. In this paper, we establish a robust approach to real-time monitoring of the *in vivo* stability of micelles using Förster Resonance Energy Transfer (FRET). This characterization method allows for exquisite insight into the fate of micellar constituents, affording the capabilities to rapidly and efficiently evaluate a library of synthetically derived micellar systems as new therapeutic platforms *in vivo*. FRET-enabled biological characterization further holds potential to tailor material systems being uniquely investigated across the delivery community towards the next generation of stable therapeutics for disease management.

Keywords

micelle; in vivo stability; delivery; FRET; self-assembly

Nanoparticles composed of block copolymers are a promising class of drug delivery systems[1–4]. Among the more widely studied are micellar blends with self-assembled amphiphilic copolymers as constituents[5–8]. These unimers allow for incorporation of hydrophobic drugs to enhance bioavailability of otherwise insoluble therapeutics, while also possessing a hydrophilic PEG corona for enhanced systemic circulation and improved biodistribution *in vivo*. However, clinical translation of these systems is limited by poor drug loadings, drug desertion and micelle disassembly upon dilution in the bloodstream, and a

[*]Prof. Paula T. Hammond, Koch Institute for Integrative Cancer Research, Department of Chemical Engineering, Massachusetts Institute of Technology, 77 Massachusetts Avenue, Cambridge, MA 02139 (USA), hammond@mit.edu.
[‡]S.W.M. and X.Z. contributed equally to this work.
The authors wish to dedicate this paper to the memory of Officer Sean Collier, for his caring service to the MIT community and for his sacrifice.
(P): 617-258-7577; (E): hammond@mit.edu; Homepage: http://web.mit.edu/hammond/lab/

Author Contributions
The manuscript was written through contributions of all authors. All authors have given approval to the final version of the manuscript.

limited understanding of the fate of micellar carriers following systemic administration[9, 10].

As a thermodynamically self-assembled structure, micelles formed on the basis of reversible, stabilizing forces such as the hydrophobic effect and electrostatics are inevitably disintegrated by a number of destabilizing mechanisms in complex biological settings. Drug desertion (“leakage”), protein adsorption, protein penetration, and dilution below the critical micelle concentration are all significant destabilizing forces upon systemic administration[10]. Furthermore, micelle size, size distribution, and surface charge impact the interactions between micelles and serum components, thereby affecting the stability and biodistribution profile of the carrier[11, 12].

Well-established *in vitro* methods[13, 14] have been introduced to determine delivery micelle stability; however, the passage of micelles through the bloodstream introduces much greater challenges due to shear forces, opsonization and uptake, and other undesirable interactions with off-target cells. It is, therefore, critical to monitor the integrity of micellar structures *in vivo*, preferably in real time. This ability allows the effective engineering of micelle carriers with desirable characteristics. Unfortunately, to date few methods exist to address this critical need[15, 16]. To clarify the mechanisms influencing serum stability of micelles and the toxicity-biodistribution relationship of micellar constituents, Förster Resonance Energy Transfer (FRET) is employed as an imaging modality to monitor association of assembled micellar carriers. FRET has proven to be a widely-used imaging tool in the biomaterials field with many applications, including sensing of temporally- and spatially-variant characteristics in biological settings (i.e. pH)[17]. This phenomena allows for exquisite resolution over dyes belonging to a FRET pair that are localized within the range of Förster distance. It is a result of non-radiative fluorescence from the excitation state of a donor dye that, upon excitation, will transfer the excitation energy to the acceptor dye, from which the resulting emission will be observed. Only in close proximity will this energy transfer occur and consequently, it indicates an intact micelle. FRET can be used alternatively as both 1) a monitor of micelle assembly and stability, and 2) as a means of monitoring drug-micelle association. Figure 1A demonstrates this concept with the FRET association of unimers in an intact empty micelle. The non-interacting unimers on the left-hand side are incapable of displaying non-radiative fluorescence transfer as a result of excitation of the donor fluorophore (blue incident arrow), resulting in donor emission (blue emission arrow); therefore, no FRET is observed. When associated as a micelle, however, excitation of the donor fluorophore (blue incident arrow) results in an electronic energy transfer that manifests as the acceptor fluorophore emission (green emission arrow), i.e. FRET. Figure 1B displays FRET association of a unimer with an encapsulated model drug, fluorophore, that acts as a FRET pair to the micelle. Non-interacting constituents (free drug and unimer comprising the micelle) on the left-hand side do not display any non-radiative fluorescence transfer as a result of excitation of the donor fluorophore (blue incident arrow), resulting in donor emission (blue emission arrow). When associated as a micelle, however, excitation of the donor fluorophore (blue incident arrow) results in an electronic energy transfer that manifests as the acceptor fluorophore emission (green emission arrow), e.g. FRET.

Applying FRET to the current study affords the ability to resolve both empty and drug-loaded micellar association in real time *in vivo*. FRET has been employed previously for *in vitro* serum stability assessments[10, 18, 19], as well as for an *in vivo* evaluation of drug stabilization of a dually encapsulated FRET pair micellar carrier[20]; however, no work to date has demonstrated the ability to track association of micellar unimers and unimer-drug association *in vivo*. Real-time monitoring of the *in vivo* fate of micelle components will be a significant advance in facilitating development of systemically-stable carriers, affording the ability to efficiently screen libraries of synthetically-derived materials for incorporation in micellar drug carriers.

The parent polymer, PEG-*b*-PPLG, was synthesized following a previously reported procedure where amine-terminated PEG was used to initiate ring opening polymerization of γ-propargyl *L*-glutamic acid N-carboxyanhydride (NCA).[21] The poly(γ-propargyl-*L*-glutamate) [PPLG] segment contains 35 repeat units, as determined by ^{1}H NMR. The PPLG block was first functionalized (approximately 70% of the pendant azide groups were reacted in this step) using copper-catalyzed alkyne-azide cycloaddition with a phenol-containing moiety, which was demonstrated to enhance the *in vitro* micelle stability under stressed conditions in a previous study[22]. Under the same conditions, the phenol-bearing block copolymer was subsequently dye-labeled at ~30% functionalization, based on NMR quantification of accessible alkyne groups and total number of dye molecules on the polymer. This translates to approximately 10 alkyne groups labeled with the near-infrared (NIR) cyanine-derived dyes, Cy5.5 and Cy7, as shown in Scheme 1, per 35 alkyne groups per polymer chain. The current dual-labeling method enabled by click chemistry allows simple modification of the core-forming block while affording minimal disturbance to the surface properties of the micelles.

Figure 2A shows the absorption and emission spectra of the NIR dye-functionalized copolymers, designated as PEG-*b*-PPLG-Cy5.5 and PEG-*b*-PPLG-Cy7 respectively. As expected, the optical properties of the copolymers are dominated by the dyes used to label the polymers. PEG-*b*-PPLG-Cy5.5 shows an absorption band with a maximum at 685 nm and an emission band at 725 nm. Compared with the spectra of PEG-*b*-PPLG-Cy5.5, both spectra of PEG-*b*-PPLG-Cy7 are red-shifted with an absorption band at a maximum at 770 nm and an emission peak at 810 nm. The good overlap between the emission spectra of PEG-*b*-PPLG-Cy5.5 and the absorption spectra of PEG-*b*-PPLG-Cy7 combined with the large separation (90 nm) between the emission bands make these two polymer-fluorophore conjugates a good FRET pair to use in the current *in vivo* study to probe the fate of micelles upon intravenous administration.

Post-functionalization of the block copolymers with the chosen NIR dyes does not impact the micelle formation properties of the block copolymers. Table 1 summarizes the size, size distribution, and ζ-potentials of the different micelle formulations. Micelles prepared from dye-labeled block copolymers in phosphate buffered saline exhibit similar sizes and zeta potentials compared to micelles of the block copolymers functionalized solely with phenol moieties. Importantly, micelles formulated using a mixture of PEG-*b*-PPLG-Cy5.5 and PEG-*b*-PPLG-Cy7, which are useful to probe the association of unimers in blank micelles, show a size of 130 nm with a slightly negative zeta potential of −0.9 mV. To investigate the

dissociation of small molecule drugs from micelles, we have prepared formulations using PEG-*b*-PPLG-Cy7 to encapsulate the small molecule dye Cy5.5 as the model drug. The size and ζ-potential of the micelles are comparable to those of micelles prepared from the polymer-fluorophore conjugates; therefore, differential *in vivo* clearance is independent of size and ζ-potential. The corresponding absorbance and emission characteristics of these micelles are presented in Figure 2B and 2C. The prepared micelles display a narrow size distribution (shown in Figure S1) with absorption characteristics consistent with the mixed dye-conjugated polymers and emission characteristics indicative of the FRET association of the mixed fluorophore-conjugated unimers or unimer-encapsulated drug fluorophore with a maximum at 800 nm.

To investigate the stability profile of the micellar structure, the empty FRET micelle concept outlined in Figure 1A was employed to probe the persistence, biodistribution, and stability fingerprint of this system. The injected micelle concentration was 0.5 mg/mL, which, upon dilution in blood [0.1mL in approximately 1.7mL total blood volume (based on 25g mouse)], is approximately 0.03 mg/mL, estimated to be 3-fold higher than the critical micelle concentration (0.01 mg/mL, based on the parent polymer[22]). Figure 3 illustrates the stability profile of this system (on the basis of FRET) following systemic administration. *In vivo* fluorescence imaging (Xenogen, Caliper Life Sciences), presented on a logarithmic scale, in Figure 3A captures micellar dissociation in real time, with increasing fluorescent signal, measured in radiant efficiency, observed from the donor channel over time relative to the FRET channel. The full panel (n = 3) for the representative data shown in Figure 3A is contained in Figure S2A. The biodistribution profile shown, on the basis of FRET, in Figure 3B is indicative of a stable system, with significant portions of the intact micelle remaining in circulation (44% recovered fluorescence) after 24h, while reduced amounts were captured in the relevant clearance organs (33% recovered fluorescence in the liver, 11% in spleen, 4% in kidneys). Biodistribution data was simultaneously collected for the donor channel and is shown in Figure S2C. It corroborates the enhanced stability of this micellar system, showing minimal donor fluorescence in the mononuclear phagocyte system (MPS) above baseline autofluorescence, thereby suggesting little dissociation.

Further, quantification of total radiant efficiency from the animal images yields a stability assessment in terms of FRET efficiency, calculated as the ratio of total radiant efficiency at the FRET channel to the sum of the total radiant efficiency from both the donor and FRET channel. Total radiant efficiency is obtained from the *in vivo* fluorescent image following background subtraction of tissue autofluorescence at the specified imaging channel pre-injection. This same calculation was performed for small volume blood samples (0.2 mL) collected at the corresponding time points for imaging. The initial condition was generated by doping blood *ex vivo* from an untreated animal and imaging it instantly upon introduction of the micellar formulation. From these data, it is clear that the micelle carrier is stable, with FRET efficiency remaining between 50–85% for up to 72 h. For reference, initial FRET efficiency of the formulation injected was 94%. Blood samples were imaged immediately upon isolation to minimize dilution effects from the anti-coagulant used to facilitate imaging. This data is displayed in Figure 3C, while analysis of the FRET efficiency (following background subtraction of the aggregate fluorescence contributions from the

untreated and individual polymer controls at the FRET channel) from the fluorescent image overlays in Figure 3A is shown in Figure S2B. The same general trends were observed for both modes of assessing micellar stability. Differences in magnitude of the FRET efficiency compiled from the images as compared to direct blood sampling are likely due to skin and tissue autofluorescence measurement interference. While investigating the association of this micellar system, persistence in circulation was also determined, on the basis of FRET, as shown in Figure 3D. The micelle was observed to be long-circulating, with a half-life of 0.12 h (fast) and 13.0 h (slow) using a two-compartment model for blood clearance.

The possibility of weak FRET association between dissociated unimers was also investigated (shown in Figure S5) by monitoring biodistribution of the fluorophore-conjugated unimers independently (injected at 0.1 mg/mL, which after dilution in blood [0.1 mL in 1.7 mL total blood volume] falls below the critical micelle concentration of 0.01 mg/mL to 0.005 mg/mL); the unimers were shown to exhibit distinctly different biodistribution profile from the micellar formulation shown in Figure 3A; therefore, it is unlikely any weak FRET association between dissociated unimers is contributing to the overall FRET signal observed. The fluorophore-conjugated polymers were also imaged at the FRET channel (Figure S6) and observed to have little contribution to fluorescence at this wavelength, further suggesting that any FRET observed *in vivo* corresponds to intact micelle.

FRET can additionally be a tool to monitor drug-micelle carrier disassociation. Encapsulating a model drug, the Cy5.5 fluorophore, as a FRET pair to the fluorophore-conjugated micelle unimer, we have characterized the ability of the micelle to retain and stabilize a model drug for delivery. Figure 4 illustrates the stability profile of this FRET drug-loaded delivery system following systemic administration. Figure 4A highlights the “leakiness” of the micelle to small molecule payloads such as the model FRET fluorophore encapsulated in this study. The full imaging panel (n = 3) is shown in Figure S3. This data was collected using *in vivo* imaging and is presented on a logarithmic scale. As evident with significantly more clearance of the intact, FRET drug-loaded micelle within the first hour post-administration, the incorporation of drug significantly impacts the micelle stability and susceptibility to clearance. This is further illustrated by the altered biodistribution relative to the empty micelle (shown in Figure 4B), as significantly more FRET signal is quantified in the mononuclear phagocyte system (53% recovered fluorescence liver-associated, 12% kidney-associated) after 8 h.

Further, calculation of the FRET efficiency from isolated blood, shown in Figure 4C, indicates only 37% remain associated with the drug carrier. To probe this drug desertion, blood was doped *ex vivo* from an untreated animal, and instantaneous exposure to blood was found to account for nearly all of this drug abandonment, as only 38% remained associated after exposure. FRET efficiency of the formulation prior to administration was 85%. The weak association of drug to the unimers comprising the current study could be due to the properties of the FRET fluorophore utilized for *in vivo* tracking. The system detailed here is tailored to more hydrophobic payloads; however, this characteristic bolus release is problematic for micellar systems and, more generally, small molecule drug delivery[23], as illustrated in the current study.

For a period up to 72 h, the FRET efficiency, shown in Figure 4C, remained near this post-administration level, oscillating between 28-40%, suggesting association of a significant portion of encapsulated dye is strong within the micelle. The circulation half-life of the drug-loaded micelle based on FRET association, shown in Figure 4D, was also investigated and found to be 0.9 h (fast) and 6.9 h (slow), based on a two-compartment blood clearance model. Further, the possibility of weak FRET association between dissociated unimers and free drug was also investigated (shown in Figure S5) by monitoring biodistribution of the fluorophore-conjugated unimers as well as free drug independently. Each exhibits distinctly different biodistribution profiles from the micellar association shown in the Figure 4A, suggesting little interference from this interaction.

From these data, it is clear that the micelle-unimer equilibrium favors micelle formation, as evidenced by the stability profile of the FRET empty micelle in Figure 3. However, incorporation of drug significantly impacts this equilibrium, as drug desertion proves problematic upon contact with blood and in a systemic environment (Figure 4). This is important to investigate as new micellar systems continue to emerge in the field with designs for better drug stability and enhanced localization in target tissue. Insight on the basis of FRET as outlined in this work can elucidate key system properties that facilitate development of more stable drug delivery vectors.

While drug chemical characteristics vary widely, this approach for understanding micelle-drug association is a powerful approach to tune specific properties of the micellar carrier to stably incorporate a particular, model therapeutic – information that can be applied to potentially a range of structurally similar therapeutics. Further, while quantitative metrics were extracted from the data collected herein, it is understood that fluorescence is largely a qualitative tool. As such, FRET remains a useful tool for validating new synthetic designs for micellar incorporation. FRET allows for rapid and efficient screening of micellar systems that are often highly tunable, where slight modifications on the unimer structure and micelle composition are important variables to investigate against its biological performance. Detailed here, several qualitative metrics are generated from small cohorts of mice, thereby allowing for a minimally-resource intensive approach for answering questions on structure-function (*in vivo*) relationships with these systems. Further, real time *in vivo* evaluation of delivery systems on the basis of FRET can be adapted broadly to a number of delivery systems being investigated, including core-shell nanoparticles, liposomes, and other self-assembled ampiphilic structures[24–27].

Conclusions

Micelles are extensively investigated as drug carriers and present exciting advantages as materials for delivery; however, a limited understanding of their fate *in vivo* has been a significant barrier to the design of systemically stable systems. The present study demonstrates an approach that uses the basis of FRET association to assess material and drug outcomes from micellar delivery systems in real time while *in vivo*, providing a means to assess colloidal carrier stability based on both the carrier biodistribution and state of assembly *in situ*. This approach can be applied to a broad variety of nanoparticle systems whereby multiple components in the system are readily labeled and assembled into a FRET

structure. As such, a number of design parameters (e.g. surface properties such as coating material, density, conformation, ζ-potential; size; composition; shape) critical to the performance of a delivery system *in vivo* can be monitored in real time, affording improved resolution of the impact of each characteristic on system performance. As the delivery community has become increasingly aware of the lack of consistency between *in vitro* and *in vivo* system performance, methodologies for direct evaluation in an in vivo setting are critical to the development of the next generation of stable therapeutics. FRET-enabled biological characterization as a robust and convenient method for developing and evaluating systems will facilitate biological screening, identifying control parameters specific to each material system being engineered for delivery. Further, the biological characterization approach detailed herein will help tailor system properties of the materials and drugs being packaged and delivered for a given therapeutic approach, enabling translation of a variety of therapeutic delivery platforms for disease management to the clinic.

Polymer Synthesis

PEG-*b*-PPLG synthesis and post functionalization

The diblock copolymer was synthesized by ring-opening polymerization of γ-propargyl-*L*-glutamate N-carboxyanhydride (NCA) initiated with the amine terminal of PEG-NH_2 (Laysan®, M_n = 5,000). The alkyne groups on the PEG-*b*-PPLG were first modified follow a previously reported procedure to achieve 70% functionalization with 4-(4-azidobutyl)phenol, a side group that was demonstrated to enhance the kinetic stability of the micelles.[1] ^{1}H NMR (400 MHz, DMF-d_7): 9.310 (s, 18H), 8.452 (br, 16H), 8.129 (s, 18H), 6.992 (br, 51H), 6.756-6.744 (br, 37H), 5.220 (m, 36H), 4.769 (s, 16H), 4.436 (s, 39H), 4.137 (s, 25), 3.588 (s, 357H), 3.503 (s, 452H), 2.513 (br, 80H), 2.201 (br, 38H), 1.863 (s, 45H), 1.547 (s, 43H). The degree of functionalization was determined from the ratio of integration at 5.220 ppm and 4.769 ppm (SI).

Dye Conjugation by Click Chemistry

Two azide-containing near-infrared (NIR) dyes in the cyanine class, named as Cy5.5 and Cy7, were purchased from Lumiprobe, LLC. Cy5.5 shows an excitation maximum at 673 nm (excitation coefficient, ε_{exc} = 209,000) and an emission maximum at 707 nm (quantum yield, Φ_{em} = 0.2). Cy7 shows an excitation maximum at 750 nm (excitation coefficient, ε_{exc} = 199,000) and an emission maximum at 773 nm (quantum yield, Φ_{em} = 0.3). The above-synthesized polymer and Cy5.5 or Cy7 (1.3 excess in mole relative to the remaining alkyne groups on the polymer chain) were dissolved in 5 ml of anhydrous DMF at r.t. in a Schlenk flask in the dark. The resulting solution was degassed with Argon for 30 min and added copper (I) bromide (20% in mole relative to the alkyne group) and N,N,N′,N″,N″-pentamethyldiethylenetriamine (PMDETA, 20% in mole relative to the alkyne group). The Schlenk flask was then sealed with a rubber septum and the reaction was stirred at r.t. in the dark for 12 h. At the end of the reaction, the reaction mixture was directly loaded on a column packed with Sephadex LH-20 gels and eluted with ~15 ml of DMF. The eluents containing the first band were collected and diluted with ~5 ml of water, which was loaded into a dialysis bag (Spectra/Por®, MWCO = 3500) and dialyzed against excess D.I. water (18.2 MΩ, 2L). The polymer-fluorophore conjugates were isolated as colored powders by

lyophilization and named as PEG-*b*-PPLG-Cy5.5 and PEG-*b*-PPLG-Cy7, respectively. Dye conjugation was performed to completion of available alkyne groups following step 1, which was 10/35 (29%) total alkyne groups on the parent polymer.

Micelle Characterization

Micelle preparation

Micelles were prepared following the procedure described previously [1]. For FRET micelles, an equal weight of both unimers were co-dissolved in DMSO to make a 10 mg/ml (total polymer concentration) solution. The micelles were then prepared by precipitating the polymer solution in 20 × (volume) of PBS. Complicated by the presence of fluorophores in the polymers, the common fluorescence method to determine the critical micelle concentration (CMC) is not applicable here. Based on the structure similarity, the CMCs of both polymer-fluorophore conjugates were estimated to be close to that of the parent polymer, which is 0.01 mg/mL.[1]

Optical Property

Beckman Coulter DU 800 UV/Vis Spectrophotometer was used to collect the absorbance and emission spectra of the polymer-fluorophore conjugates and micelle formulations using rectangular cuvettes with a 1-cm light path.

Micelle Properties

Dynamic light scattering and zeta potential measurements were performed using a Delsa™ particle size analyzer (Beckman Coulter Inc.). All the measurements were carried out at 25°C in 10mM NaCl in DI water at a concentration of 0.1 mg/mL. The sample solutions were purified by passing through a Millipore 0.45 μm filter. The scattered light of a vertically polarized He-Ne laser (532 nm) was measured at an angle of 165° and was collected on an auto-correlator.

In vivo experimentation

NCr nude homozygous female mice (Taconic) were used for *in vivo* imaging (IVIS, Xenogen) and biodistribution experimentation. BALB/c female mice (Taconic) were used to collect circulation and FRET efficiency data. All mice were given an alfalfa-free diet (AIN-93, PharmaServ) one-week prior to experimentation and remained on the diet for the duration of imaging. Micellar formulations, diluted in PBS, were administered systemically via the tail vein in 0.1 mL injections (~1×10^9 in total radiant efficiency at the FRET channel, corresponding to a 0.5 mg/mL injection of materials for FRET micellar systems; 0.1 mg/mL for “unimers” so the micelles would dissociate rapidly upon injection due to dilution below CMC of 0.01 mg/mL). IVIS live-animal fluorescence imaging (exposure ‘1 second’, binning ‘medium’, field of view ‘D’, fstop ‘2’) was employed for micelle tracking up to 96 h at the following fluorescent channels: donor (λ_{ex} = 640 nm; λ_{em} = 700 nm); acceptor (λ_{ex} = 745 nm; λ_{em} = 800 nm); FRET (λ_{ex} = 640 nm; λ_{em} = 800 nm). Necropsy and examination of biodistribution was performed at 8 h (drug-loaded micelle) and 24 h (empty FRET micelle). Blood (~0.9 mL, half total blood volume) was collected via cardiac puncture, followed by harvesting of the liver, spleen, kidneys, heart, and lungs. IVIS imaging was conducted to

quantify recovered fluorescence following background subtraction of auto-fluorescence from corresponding tissue and blood samples of an untreated animal. Live animal blood sampling was performed via retro-orbital bleeding. Blood samples were diluted upon collection in 0.5 M EDTA to prevent coagulation. IVIS imaging of the blood was conducted immediately upon isolation (to minimize further dilution effects on FRET association) to quantify recovered fluorescence. Blood from an untreated animal was used for background subtraction to perform subsequent calculations regarding FRET efficiency, ε_{FRET} [calculated as the ratio of signal collected from the FRET channel (λ_{ex} = 640 nm; λ_{em} = 800 nm) to that at the donor channel (λ_{ex} = 640 nm; λ_{em} = 700 nm)] and micelle persistence in circulation [based on FRET, λ_{ex} = 640 nm; λ_{em} = 800 nm; calculated as a % recovered fluorescence from the administered dose].

All quantification of fluorescence recovery from animal imaging is presented as radiant efficiency, which is the ratio of radiant flux to input electrical power. This value is obtained from the Living Image Software (Caliper Life Sciences, PerkinElmer) following region of interest identification of the fluorescence desired for quantification. All measurements were normalized to tissue auto-fluorescence for accurate representation of the delivery system-associated fluorescence. Images presented in panel format were normalized against a “pre” image from which the minimum and maximum values for radiant efficiency were set to visualize this change in fluorescence following systemic introduction of material.

Supplementary Material

Refer to Web version on PubMed Central for supplementary material.

Acknowledgments

The authors would like to acknowledge the David H. Koch Institute for Integrative Cancer Research at MIT for its gracious support and use of facilities, including the Swanson Biotechnology Center supported by the Koch Institute Support (core) Grant P30-CA14051 from the National Cancer Institute. The authors would also like to thank funding from the internal David H. Koch Nanoparticle grant and the NIH Challenge grant 5 U54 CA151884-02 (CCNE) that funded this work. S.W.M. would also like to acknowledge a National Science Foundation Graduate Research Fellowship (N.S.F. G.R.F.).

ABBREVIATIONS

FRET Förster Resonance Energy Transfer

References

1. Davis ME, Chen Z, Shin DM. Nanoparticle therapeutics: an emerging treatment modality for cancer. Nat Rev Drug Discov. 2008; 7:771–782. [PubMed: 18758474]
2. Duncan R. The dawning era of polymer therapeutics. Nat Rev Drug Discov. 2003; 2:347–360. [PubMed: 12750738]
3. Torchilin VP. Micellar nanocarriers: Pharmaceutical perspectives. Pharmaceut Res. 2007; 24:1–16.
4. Shi JJ, Xiao ZY, Kamaly N, Farokhzad OC. Self-Assembled Targeted Nanoparticles: Evolution of Technologies and Bench to Bedside Translation. Acc Chem Res. 2011; 44:1123–1134. [PubMed: 21692448]
5. Cabral H, Nishiyama N, Kataoka K. Supramolecular Nanodevices: From Design Validation to Theranostic Nanomedicine. Acc Chem Res. 2011; 44:999–1008. [PubMed: 21755933]

6. Kataoka K, Harada A, Nagasaki Y. Block copolymer micelles for drug delivery: design, characterization and biological significance. Adv Drug Deliv Rev. 2001; 47:113–131. [PubMed: 11251249]
7. Mikhail AS, Allen C. Block copolymer micelles for delivery of cancer therapy: Transport at the whole body, tissue and cellular levels. J Control Release. 2009; 138:214–223. [PubMed: 19376167]
8. Gaucher G, Dufresne MH, Sant VP, Kang N, Maysinger D, Leroux JC. Block copolymer micelles: preparation, characterization and application in drug delivery. J Control Release. 2005; 109:169–188. [PubMed: 16289422]
9. Bae YH, Yin HQ. Stability issues of polymeric micelles. J Control Release. 2008; 131:2–4. [PubMed: 18625275]
10. Kim S, Shi Y, Kim JY, Park K, Cheng JX. Overcoming the barriers in micellar drug delivery: loading efficiency, in vivo stability, and micelle-cell interaction. Expert Opin Drug Deliv. 2010; 7:49–62. [PubMed: 20017660]
11. Alexis F, Pridgen E, Molnar LK, Farokhzad OC. Factors affecting the clearance and biodistribution of polymeric nanoparticles. Mol Pharm. 2008; 5:505–515. [PubMed: 18672949]
12. Yamamoto Y, Nagasaki Y, Kato Y, Sugiyama Y, Kataoka K. Long-circulating poly(ethylene glycol)-poly(D,L-lactide) block copolymer micelles with modulated surface charge. J Control Release. 2001; 77:27–38. [PubMed: 11689257]
13. Savic R, Luo LB, Eisenberg A, Maysinger D. Micellar nanocontainers distribute to defined cytoplasmic organelles. Science. 2003; 300:615–618. [PubMed: 12714738]
14. Murakami M, Cabral H, Matsumoto Y, Wu SR, Kano MR, Yamori T, et al. Improving Drug Potency and Efficacy by Nanocarrier-Mediated Subcellular Targeting. Sci Transl Med. 2011; 3:ra2.
15. Lee H, Hoang B, Fonge H, Reilly RM, Allen C. In Vivo Distribution of Polymeric Nanoparticles at the Whole-Body, Tumor, and Cellular Levels. Pharmaceut Res. 2010; 27:2343–2355.
16. Liu JB, Zeng FQ, Allen C. In vivo fate of unimers and micelles of a poly(ethylene glycol)-block-poly(caprolactone) copolymer in mice following intravenous administration. Eur J Pharm Biopharm. 2007; 65:309–319. [PubMed: 17257817]
17. Jares-Erijman EA, Jovin TM. FRET imaging. Nature Biotechnology. 2003; 21:1387–1395.
18. Chen H, Kim S, Li L, Wang S, Park K, Cheng JX. Release of hydrophobic molecules from polymer micelles into cell membranes revealed by Forster resonance energy transfer imaging. Proc Natl Acad Sci U S A. 2008; 105:6596–6601. [PubMed: 18445654]
19. Jiwpanich S, Ryu JH, Bickerton S, Thayumanavan S. Noncovalent encapsulation stabilities in supramolecular nanoassemblies. J Am Chem Soc. 2010; 132:10683–10685. [PubMed: 20681699]
20. Chen H, Kim S, He W, Wang H, Low PS, Park K, et al. Fast release of lipophilic agents from circulating PEG-PDLLA micelles revealed by in vivo Forster resonance energy transfer imaging. Langmuir. 2008; 24:5213–5217. [PubMed: 18257595]
21. Engler AC, Lee HI, Hammond PT. Highly Efficient "Grafting onto" a Polypeptide Backbone Using Click Chemistry. Angew Chem Int Ed Engl. 2009; 48:9334–9338. [PubMed: 19902445]
22. Zhao XY, Poon Z, Engler AC, Bonner DK, Hammond PT. Enhanced Stability of Polymeric Micelles Based on Postfunctionalized Poly(ethylene glycol)-b-poly(gamma-propargyl L-glutamate): The Substituent Effect. Biomacromolecules. 2012; 13:1315–1322. [PubMed: 22376183]
23. Chen Z. Small-molecule delivery by nanoparticles for anticancer therapy. Trends Mol Med. 2010; 16:594–602. [PubMed: 20846905]
24. Hamley IW. Self-assembly of amphiphilic peptides. Soft Matter. 2011; 7:4122–4138.
25. Trent A, Marullo R, Lin B, Black M, Tirrell M. Structural properties of soluble peptide amphiphile micelles. Soft Matter. 2011; 7:9572–9582.
26. Chung EJ, Cheng Y, Morshed R, Nord K, Han Y, Wegscheid ML, et al. Fibrin-binding, peptide amphiphile micelles for targeting glioblastoma. Biomaterials. 2014; 35:1249–1256. [PubMed: 24211079]
27. Aida T, Meijer EW, Stupp SI. Functional supramolecular polymers. Science. 2012; 335:813–817. [PubMed: 22344437]

References

1. Zhao XY, Poon Z, Engler AC, Bonner DK, Hammond PT. Biomacromolecules. 2012; 13(5):1315–1322. [PubMed: 22376183]

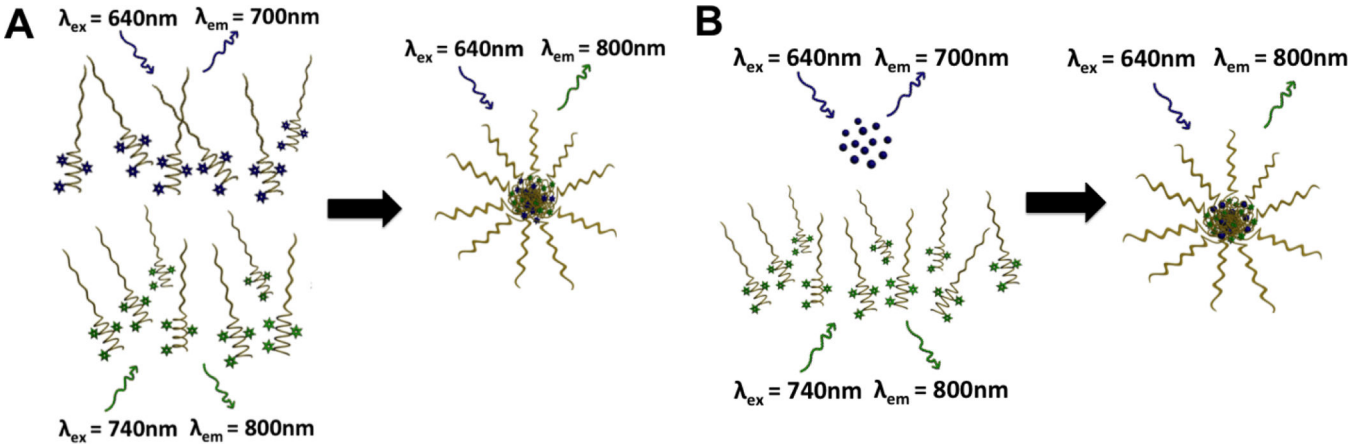

Figure 1. FRET concept for assessing biological performance

(A) FRET micelle prepared on the basis of independently fluorophore-conjugated unimers mixed in equivalent ratio. **(B)** FRET drug-loaded micelle prepared on the basis of fluorophore-conjugated unimers with an encapsulated, FRET pair model drug.

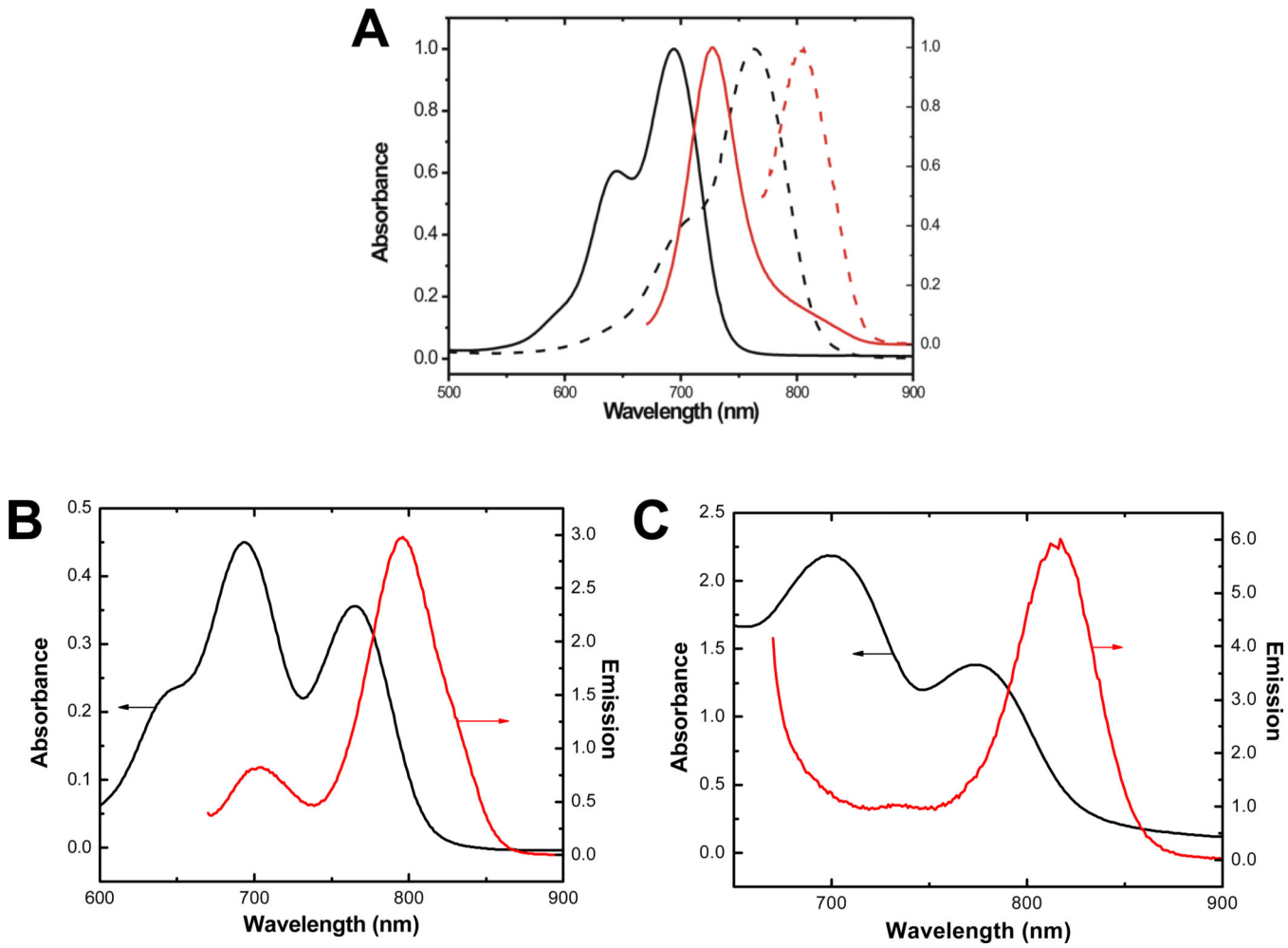

Figure 2.

(A) Normalized absorbance (black) and emission (red) spectra for the polymer-fluorophore conjugates. PEG-*b*-PPLG-Cy5.5 (solid line) and PEG-*b*-PPLG-Cy7 (dotted line). **(B)** Absorbance and emission spectra for FRET-assembled empty micelle [PEG-*b*-PPLG-Cy5.5 + PEG-*b*-PPLG-Cy7]. **(C)** Absorbance and emission spectra for FRET-assembled drug-loaded micelle [Cy5.5 + PEG-*b*-PPLG-Cy7].

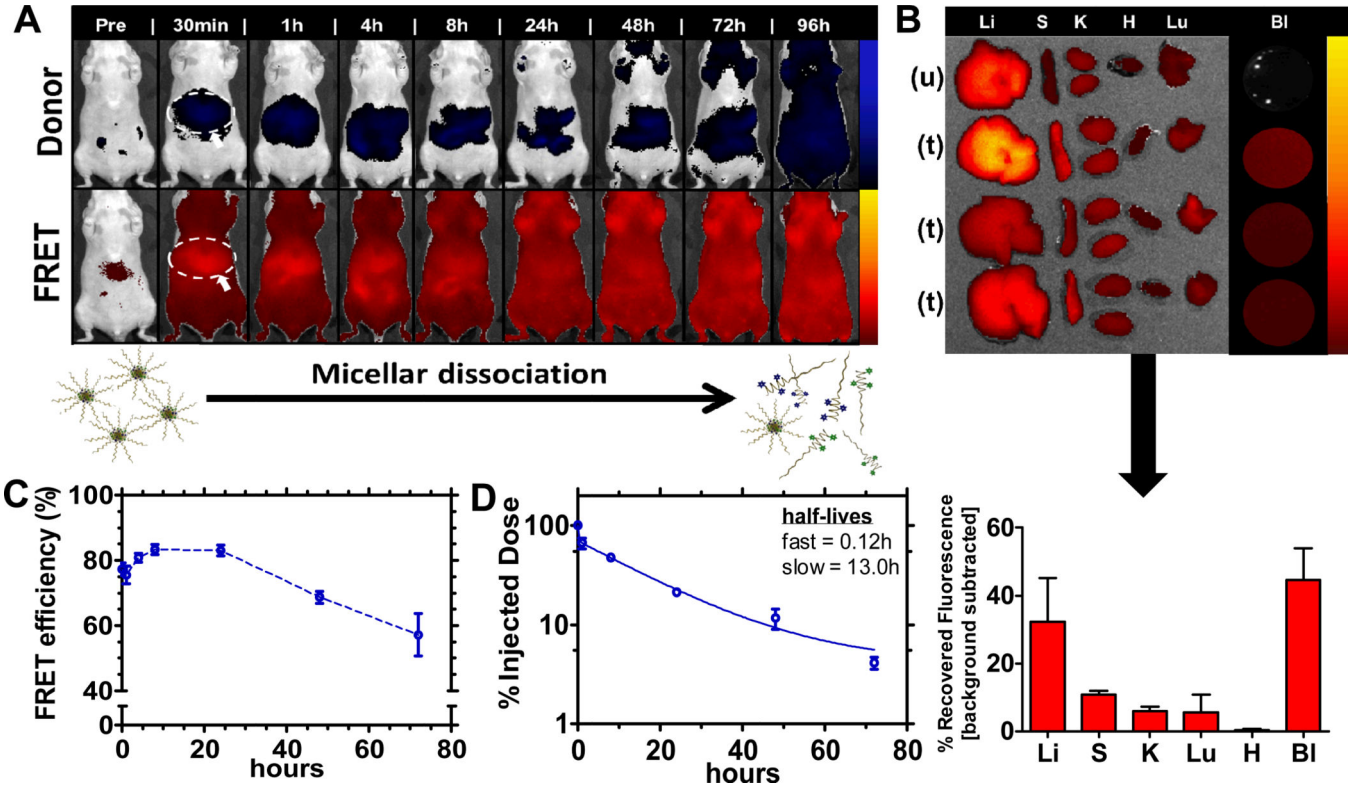

Figure 3. FRET empty micelle formulation

(A) Biodistribution of FRET empty micelles using IVIS imaging. Top row corresponds to the donor fluorescent channel, λ_{ex} = 640 nm, λ_{em} = 700 nm; bottom row corresponds to FRET fluorescent channel, λ_{ex} = 640 nm; λ_{em} = 800 nm. Liver association is identified (circle and arrow) in the first image displayed post-systemic administration for reference. Full panel (n = 3) shown in Figure S2. **(B)** Biodistribution after 24 h (n = 3). Images correspond to the FRET channel, λ_{ex} = 640 nm, λ_{em} = 800 nm. Liver (Li), Spleen (S), Kidneys (K), Heart (H), Lungs (Lu), and Blood (Bl) extracted for each FRET micelle treatment and an untreated control for autofluorescence background. Below the image is quantification of recovered fluorescence (units of radiant efficiency) following background subtraction of autofluorescence from the untreated control. **(C)** FRET efficiency of micelles in circulation as a function of time (determined from live-animal bleeds following systemic administration). Initial FRET efficiency reported as that obtained immediately following doping of blood collected from an untreated animal with the micellar formulation. Data represents mean +/− SEM. **(D)** Circulation profile of FRET empty micelles, displaying percent of injected dose recovered as a function of time. Raw data shown in Figure S4. Data represents mean +/− SEM.

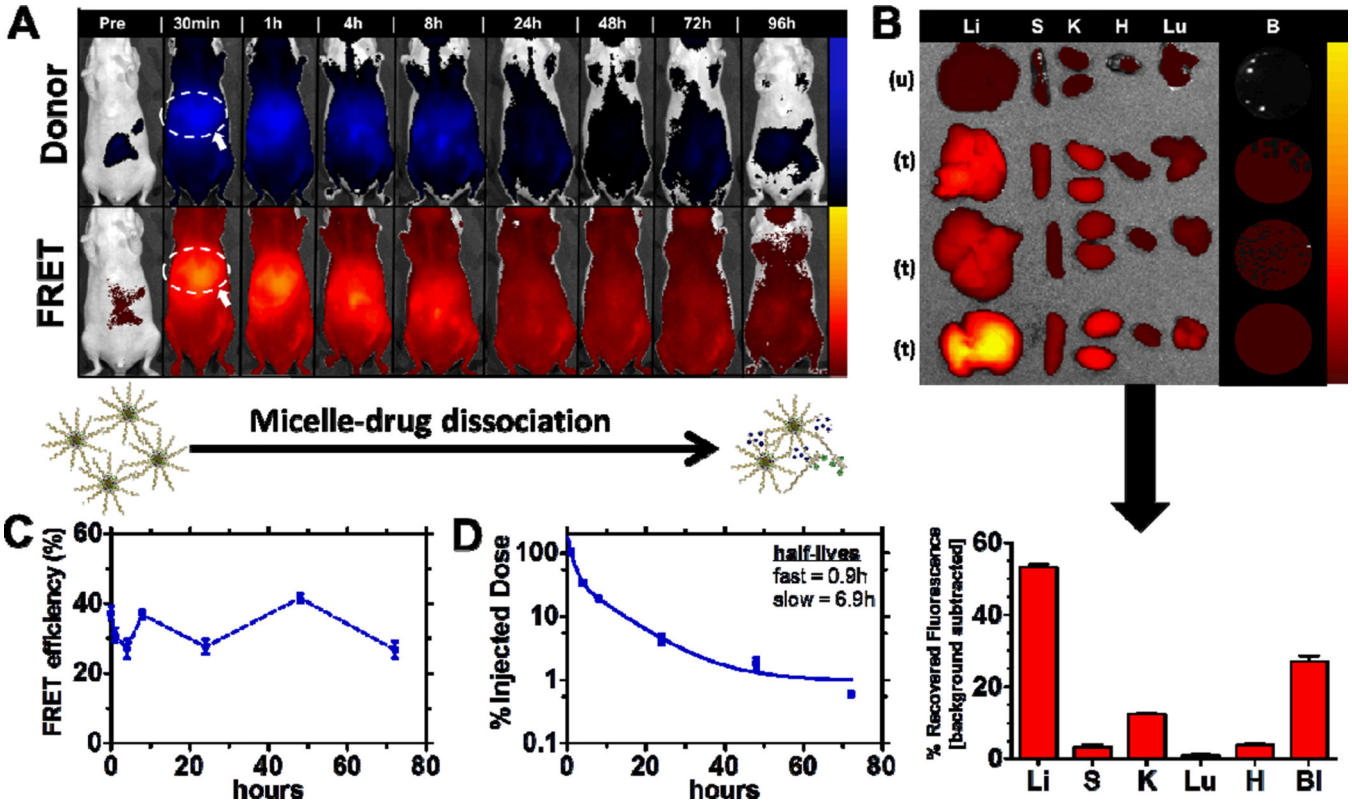

Figure 4. FRET drug-loaded micelles

(A) Biodistribution of FRET drug-loaded micelles using IVIS imaging. Top row corresponds to the donor fluorescent channel, λ_{ex} = 640 nm, λ_{em} = 700 nm; bottom row corresponds to FRET fluorescent channel, λ_{ex} = 640 nm; λ_{em} = 800nm. Liver association is identified (circle and arrow) in the first image displayed post-systemic administration for reference. Full panel (n = 3) shown in Figure S3. **(B)** Biodistribution after 8 h (n = 3). Images correspond to the FRET channel, λ_{ex} = 640 nm, λ_{em} = 800 nm. Liver (Li), Spleen (S), Kidneys (K), Heart (H), Lungs (Lu), and Blood (Bl) extracted for each FRET drug-loaded micelle treatment and an untreated control for autofluorescence background. Below the image is quantification of recovered fluorescence (units of radiant efficiency) following background subtraction of autofluorescence from the untreated control. **(C)** FRET efficiency of drug-loaded micelles in circulation as a function of time (determined from live-animal bleeds following systemic administration). Initial FRET efficiency reported as that obtained immediately following doping of blood collected from an untreated animal with the micelle formulation. Data represents mean +/− SEM. **(D)** Circulation profile of FRET drug-loaded micelles, displaying percent of injected dose fluorescence recovered as a function of time. Raw data shown in Figure S4. Data represents mean +/− SEM.

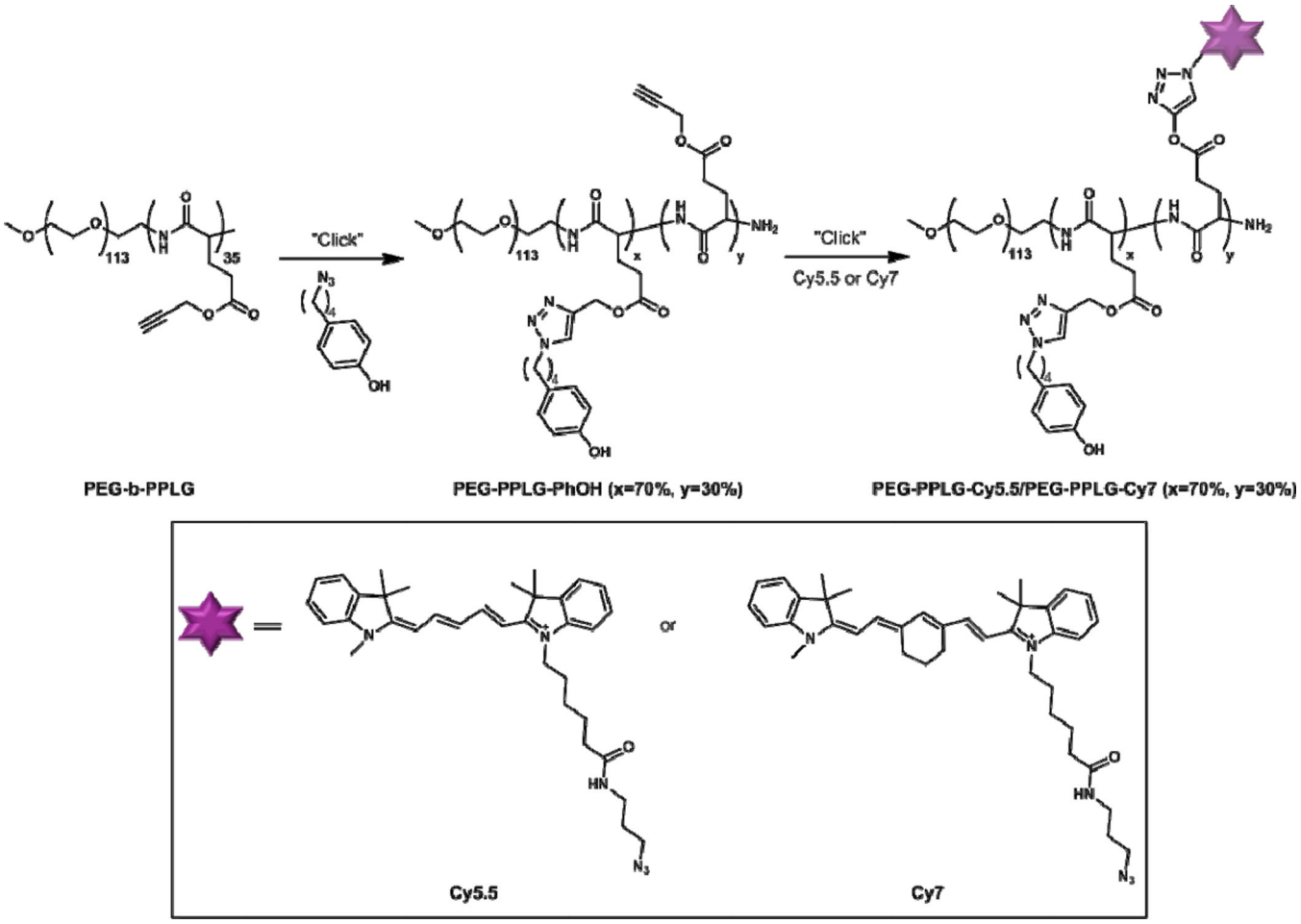

Scheme 1.
Synthesis of FRET-paired unimers for micellar assembly.

Table 1

Dynamic light scattering and ζ potential analysis of micellar components and FRET micelle formulations, performed in phosphate buffered saline at 25 °C.

FRET micelle	d_h/ nm	PDI	ζ potential / mV
PEG-*b*-PPLG$_{Cy5.5}$	121	0.13	−1.9
PEG-*b*-PPLG$_{Cy7}$	134	0.20	−4.7
PEG-*b*-PPLG$_{Cy5.5}$ + PEG-*b*-PPLG$_{Cy7}$	130	0.11	−0.9
Cy5.5 encapsulated PEG-*b*-PPLG$_{Cy7}$	129	0.18	−2.8